Supplemental Material for: Emergent c-axis magnetic helix in manganite-nickelate superlattices

G. Fabbris,[1,2,*] N. Jaouen,[3] D. Meyers,[1] J. Feng,[4] J. D. Hoffman,[5,6] R. Sutarto,[7] S. G. Chiuzbăian,[4,3] A. Bhattacharya,[5,6] and M. P. M. Dean[1,†]

[1]*Department of Condensed Matter Physics and Materials Science, Brookhaven National Laboratory, Upton, New York 11973, USA*
[2]*Advanced Photon Source, Argonne National Laboratory, Argonne, Illinois 60439, USA*
[3]*Synchrotron SOLEIL, L'Orme des Merisiers, Saint-Aubin, BP 48, 91192 Gif-sur-Yvette, France*
[4]*Sorbonne Universités, UPMC Univ. Paris 06, UMR 7614, Laboratoire de Chimie Physique-Matière et Rayonnement, 11 rue Pierre et Marie Curie, F-75005 Paris, France*
[5]*Materials Science Division, Argonne National Laboratory, Argonne, Illinois 60439, USA*
[6]*Nanoscience and Technology Division, Argonne National Laboratory, Argonne, Illinois 60439, USA*
[7]*Canadian Light Source, University of Saskatchewan, Saskatoon, Saskatchewan S7N 2V3, Canada*

(Dated: October 9, 2018)

This document provides supporting evidence for the main manuscript. Section I provides further details on the procedures used to analyze the x-ray resonant magnetic reflectivity (XRMR) data. The x-ray absorption spectroscopy (XAS) and x-ray magnetic circular dichroism (XMCD) data collected at the O K-, Mn $L_{3,2}$- and Ni L_2-edges are reported in section II. In section III, the Ni L_3-edge RIXS of $(LSMO)_9/(LNO)_3$ is further compared with atomic calculations that assume a small broadening as well as a mixture of Ni $3d^8$ and $3d^7$ configurations. Section IV provides x-ray reflectivity and surface x-ray diffraction measurements that demonstrate the $(La_{2/3}Sr_{1/3}MnO_3)_9/(LaNiO_3)_3$ [$(LSMO)_9/(LNO)_3$] high sample quality.

I. FURTHER DETAILS ON THE XRMR ANALYSIS

The XRMR was modeled using the magnetic matrix formalism by stacking layers of $La_{2/3}Sr_{1/3}O$, MnO_2, LaO and NiO_2 to reproduce the 14x[$(LSMO)_9/(LNO)_3$] heterostructure. Additionally, a top layer of oxygen was added to account for a small amount of contaminants on the film surface.[1] Each layer has eight parameters: thickness, roughness, charge optical constants (δ and β), magnetic optical constants (δ_m and β_m), and the angles of the magnetic moment around (γ) and with respect to (ϕ) the surface normal (see Ref. 2 for more details). A major difficulty of the XRMR analysis is constraining this large number of parameters, which we addressed in the following manner. The thickness and roughness of $La_{2/3}Sr_{1/3}O$ and MnO_2 as well as LaO and NiO_2 were set to be the same. We also used off-resonant soft x-ray reflectivity measured at energies near the Ni L_2 (at 890 eV) and Mn L_3 (at 630 eV) to constrain the thickness and roughness during the on-resonance fitting. Both charge and magnetic optical constants were retrieved from XAS and XMCD measurements at the Ni $L_{3,2}$-, Mn $L_{3,2}$-, and La M_4-edges (see Fig. S2). The magnetic moment angles were then set according to different models.

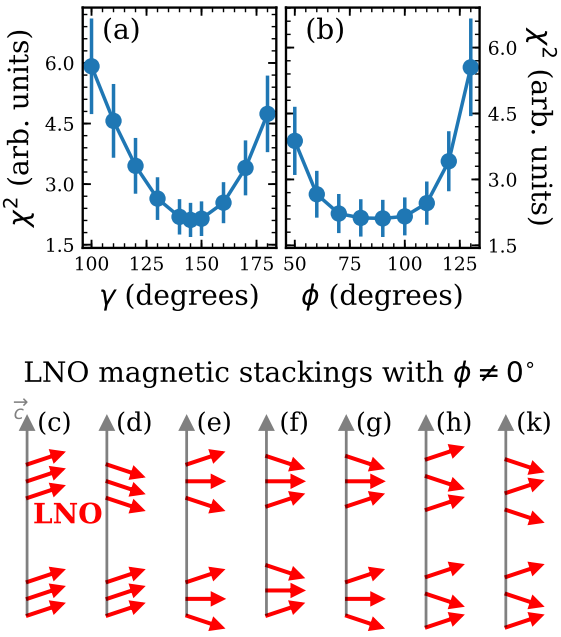

FIG. S1. (a)&(b) Ni L_2-edge XRMR χ^2 as a function of the coupling angle between $(LSMO)_9$ layers (γ) and the angle of Ni moments with respect to the c-axis [ϕ, using the structure in panel (c)], respectively. (c) through (k) show the various out-of-plane $(LNO)_3$ magnetic structures that were also tested. Within the estimated uncertainty, the magnetic structure with in-plane NiO_2 moment best reproduces the data.

Even with the constraints described above, it is impractical to fit the optical constants which were kept fixed. We note, however, that best fits were obtained by rescaling the magnetic optical constants. At the Ni L_2-edge these were rescaled by a factor of 0.8. The situation is more complex at the Mn L_3 since the charge transfer drives an inhomogeneous magnetization. In this case the best models include a factor of 0.3 for the first two MnO_2

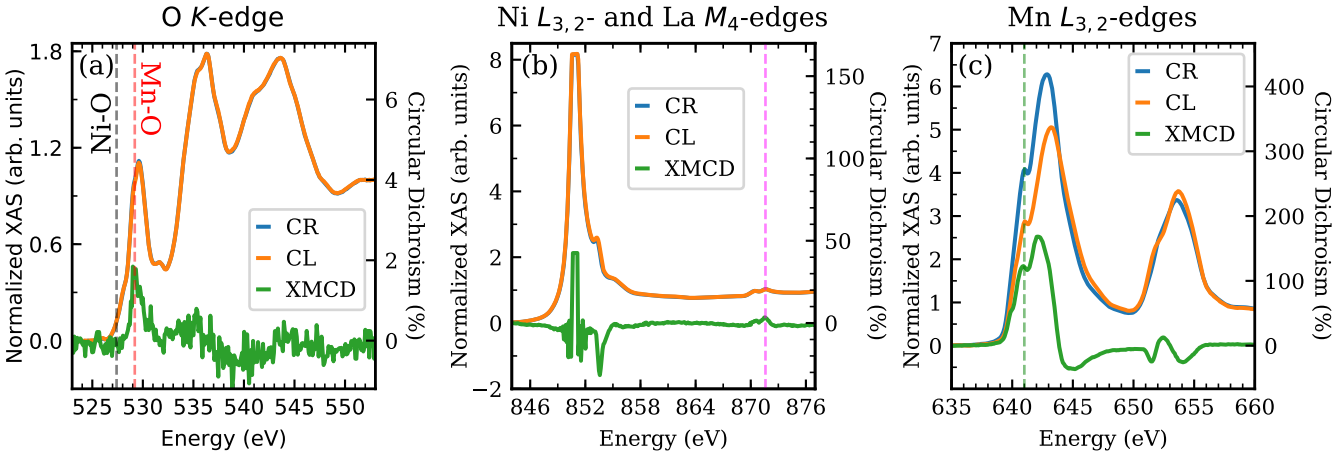

FIG. S2. XAS and XMCD collected at the (a) O K-, (b) La M_4- and Ni $L_{3,2}$-, as well as Mn (c) $L_{3,2}$-edges of the $(LSMO)_9/(LNO)_3$ heterostructure. On panel (a), the vertical dashed lines mark the resonant energy of the Ni-O (black) and Mn-O (red) ligand holes. On panels (b)&(c) the dashed lines correspond to the incident x-ray energy used in the data shown on Fig. 3 of the main manuscript.

at each interface and a factor of 0.9 for the remaining five layers. We also point out that the charge transfer also implies that distinct charge optical constants are likely needed for the MnO_2 at the interfaces, however attempts to use the simulated XAS of Mn^{4+} as a reference did not yield better results.

We initially attempted to adjust the thickness, roughness, and magnetic moment angles using both the Levenberg-Marquardt and simplex methods,[2,3] but the magnetic angles always converged to local minima of χ^2. We thus determine the optimal magnetic angles by separately fixing each angle and collecting the resulting χ^2 of the XRMR asymmetry. Some of the results of this procedure can be seen in Fig. S1. Given the complexity of these methods and the number of parameters described above, it is particularly difficult to estimate the error on the magnetic angles. Based on Fig. S1 (a)&(b) we estimate $\Delta\gamma \sim 20°$ and $\Delta\phi \sim 30°$. In the manuscript, we show our attempts to model the $(LNO)_3$ magnetic order by varying the γ of each NiO_2 layer [Fig. 3(e)]. We also investigated models with varying ϕ as sketched in Fig. S1(c)-(k), but these yield worse χ^2.

II. X-RAY ABSORPTION SPECTROSCOPY AND X-RAY MAGNETIC CIRCULAR DICHROISM

XAS and XMCD measurements at the O K-, Mn $L_{3,2}$-, Ni $L_{3,2}$-, and La M_4-edges of $(LSMO)_9/(LNO)_3$ were performed at the REIXS beamline of the Canadian Light Source. The data were collected in total electron yield mode and at 25 K. A permanent magnet with a field of 0.6 T was applied and then removed at low temperature, the measurement was thus performed on remanence. The results are displayed in Fig. S2. While the O K-edge XAS pre-edge is dominated by signal from oxygen ligand holes, the post-edge oscillations are related to both the density of empty states far above the Fermi energy and the photoelectron multiple scattering, thus being less relevant to the current investigation. Comparing the XAS and XMCD signal at the Ni L_2-edge with the literature suggests an average valence within 2.1+ to 2.3+.[4,5] Such hole doping level is also consistent with the absence of fluorescence signal in the Ni L_3-edge RIXS (Fig. S4

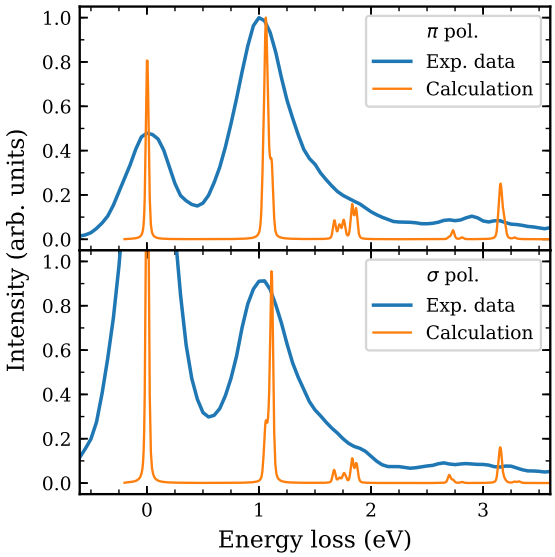

FIG. S3. The RIXS spectra collected at the Ni L_3-edge (853.5 eV) of $(LSMO)_9/(LNO)_3$ is compared with atomic calculations. Small lifetime and resolution broadening were used in order to highlight the many multiplets excitations that are present in the $3d^8$ configuration.

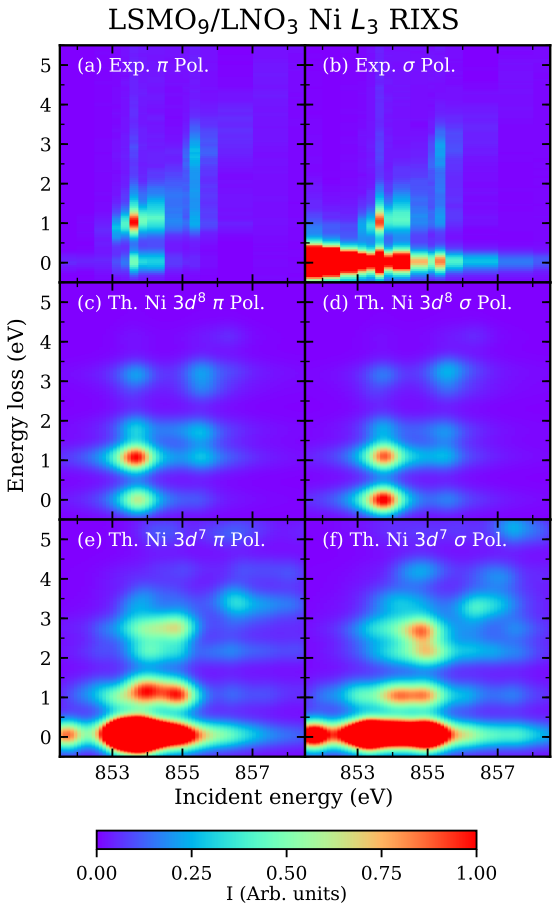

FIG. S4. (a)&(b) display the experimental Ni L_3-edge RIXS data of $LSMO_9/LNO_3$ collected with π and σ incident x-ray polarization, respectively. Atomic simulations of Ni $3d^8$ and $3d^7$ RIXS are shown in panels (c)&(d) and (e)&(f), respectively.

(a)&(b)) that is seen in $La_{4/3}Sr_{2/3}NiO_4$ ($Ni^{2.33+}$).[6] The data for the Mn $L_{3,2}$-edges are also consistent with previous results.[7] The Ni and Mn XAS and XMCD displayed in Fig. S2 were combined with non-resonant tabulated optical constants[8] to generate the complex index of refraction used in the XRMR simulations. The XRMR fits shown in the main manuscript were performed at the incident x-ray energies marked by the dashed lines in Fig. S2 (b)&(c).

The XMCD signal carries information on the atomic magnetic moment that can be extracted using sum rules.[9] This analysis is rather straightforward at the Mn $L_{3,2}$-edges, yielding a total magnetic moment of 3.03 μ_B/Mn. Analysis of the Ni $L_{3,2}$-edges is much more complicated because the La M_4-edge largely overlaps with the Ni L_3 [Fig. S2 (b)]. This issue is known to generate large uncertainties, for instance sum rules analysis of La_2NiMnO_6 finds a total moment of 0.74 μ_B/Ni, about half of what is expected from calculations ($\sim 1.42\mu_B$/Ni).[10] Our analysis yield 0.25 μ_B/Ni for $(LSMO)_9/(LNO)_3$, similar to the 0.2-0.5 μ_B/Ni found in [111]-grown $(LaMnO_3)_n/(LaNiO_3)_n$ superlattices that contain ferromagnetic NiO_2 planes.[11] Given the substantial uncertainty in this extracted magnetic moment, any analysis of its implication to the magnetic ordering within the NiO_2 planes of $(LSMO)_9/(LNO)_3$ would be largely speculative.

III. ATOMIC SIMULATIONS OF NI L-EDGE RIXS

Determining the specific types of excitations involved in each peak observed in Fig. S4 (a)&(b) is difficult, since the Ni $3d^8$ leads to 35 different multiplets in D_{4h} point

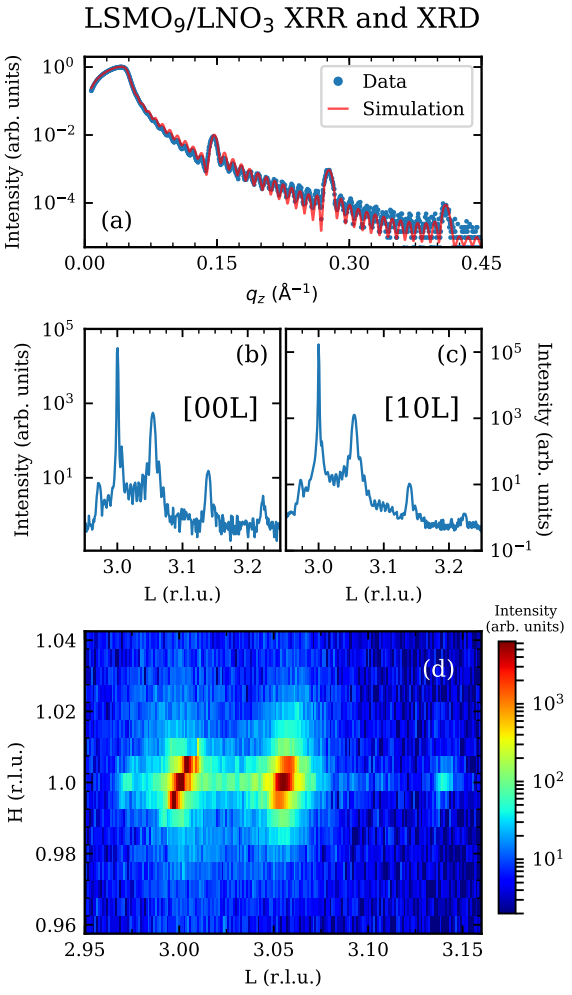

FIG. S5. $(LSMO)_9/(LNO)_3$ superlattice characterization. (a) XRR data together with a simulation that uses the same structural model as that used in the x-ray resonant magnetic reflectivity reported in the main text. (b)&(c) XRD scans along [00L] and [10L] directions, respectively. (d) 2D XRD data around the (103) reflection. The substrate's reciprocal lattice is used are a reference, thus the sharp peaks at (003) and (103) are from $SrTiO_3$.

group symmetry. This is illustrated in Fig. S3, where we plot the RIXS spectrum collected at 853.5 eV incident energy together with RIXS calculations using the same parameters described in the manuscript but with an artificially small broadening. Note that even the first peak at $\sim$ 1 eV is actually composed by ^3E_g and $^3B_{2g}$ excitations (in D_{4h} symmetry), in which holes populate the orbitals $3d^1_{yz/zx}$ $3d^1_{x^2-y^2}$ and $3d^1_{xy}$ $3d^1_{3z^2-r^2}$ respectively.

Figure S4 displays the Ni L_3 RIXS data of $(LSMO)_9/(LNO)_3$ together with atomic calculations using Ni $3d^8$ and $3d^7$ as ground states. These results clearly demonstrate that the $(LNO)_3$ layers are dominated by Ni $3d^8$ ions. The experimental result is also markedly distinct from the broad diagonal feature observed in RENiO$_3$ (RE = La and Nd).[12,13]

IV. SAMPLE CHARACTERIZATION

The $LSMO_9/LNO_3$ superlattice studied in the main manuscript was previously investigated in Ref. 14. Nevertheless, we have performed x-ray reflectivity (XRR) and surface x-ray diffraction (XRD) measurements to further confirm the sample quality. Data was collected at room temperature using Cu K_α radiation from a Brüker D8 Discover equipment. The results are displayed in Fig. S5. Both XRR and XRD measurements show well defined finite thickness fringes and superlattice peaks that are consistent with a good quality sample. Additionally, Figure S5 (d) demonstrate that the superlattice *ab* plane is strained to the $SrTiO_3$ substrate.

* gfabbris@anl.gov
† mdean@bnl.gov

[1] Jorge E Hamann-Borrero, Sebastian Macke, Woo Seok Choi, Ronny Sutarto, Feizhou He, Abdullah Radi, Ilya Elfimov, Robert J Green, Maurits W Haverkort, Volodymyr B Zabolotnyy, Ho Nyung Lee, George A Sawatzky, and Vladimir Hinkov, "Valence-state reflectometry of complex oxide heterointerfaces," npj Quantum Materials **1**, 16013 (2016).

[2] S. Macke and E. Goering, "Magnetic reflectometry of heterostructures," Journal of Physics: Condensed Matter **26**, 363201 (2014).

[3] M. Elzo, E. Jal, O. Bunau, S. Grenier, Y. Joly, A. Y. Ramos, H. C. N. Tolentino, J. M. Tonnerre, and N. Jaouen, "X-ray resonant magnetic reflectivity of stratified magnetic structures: Eigenwave formalism and application to a W/Fe/W trilayer," Journal of Magnetism and Magnetic Materials **324**, 105–112 (2012).

[4] J. van Elp, B. G. Searle, G. A. Sawatzky, and M. Sacchi, "Ligand hole induced symmetry mixing of d^8 states in $Li_xNi_{1x}O$, as observed in Ni $2p$ x-ray absorption spectroscopy," Solid State Communications **80**, 67–71 (1991).

[5] M. Abbate, F. M. F. de Groot, J. C. Fuggle, A. Fujimori, Y. Tokura, Y. Fujishima, O. Strebel, M. Domke, G. Kaindl, J. van Elp, B. T. Thole, G. A. Sawatzky, M. Sacchi, and N. Tsuda, "Soft-x-ray-absorption studies of the location of extra charges induced by substitution in controlled-valence materials," Physical Review B **44**, 5419–5422 (1991).

[6] G. Fabbris, D. Meyers, L. Xu, V. M. Katukuri, L. Hozoi, X. Liu, Z.-Y. Chen, J. Okamoto, T. Schmitt, A. Uldry, B. Delley, G. D. Gu, D. Prabhakaran, A. T. Boothroyd, J. van den Brink, D. J. Huang, and M. P. M. Dean, "Doping Dependence of Collective Spin and Orbital Excitations in the Spin-1 Quantum Antiferromagnet $La_{2-x}Sr_xNiO_4$ Observed by X Rays," Physical Review Letters **118**, 156402 (2017).

[7] C. Aruta, G. Ghiringhelli, V. Bisogni, L. Braicovich, N. B. Brookes, A. Tebano, and G. Balestrino, "Orbital occupation, atomic moments, and magnetic ordering at interfaces of manganite thin films," Physical Review B **80**, 014431 (2009).

[8] C. T. Chantler, "Theoretical Form Factor, Attenuation, and Scattering Tabulation for Z =192 from E =110 eV to E =0.41.0 MeV," Journal of Physical and Chemical Reference Data **24**, 71–643 (1995).

[9] Paolo Carra, B. T. Thole, Massimo Altarelli, and Xindong Wang, "X-ray circular dichroism and local magnetic fields," Physical Review Letters **70**, 694–697 (1993).

[10] Haizhong Guo, Arunava Gupta, Maria Varela, Stephen Pennycook, and Jiandi Zhang, "Local valence and magnetic characteristics of La_2NiMnO_6," Physical Review B **79**, 172402 (2009).

[11] C. Piamonteze, M. Gibert, J. Heidler, J. Dreiser, S. Rusponi, H. Brune, J.-M. Triscone, F. Nolting, and U. Staub, "Interfacial properties of $LaMnO_3/LaNiO_3$ superlattices grown along (001) and (111) orientations," Physical Review B **92**, 014426 (2015).

[12] Valentina Bisogni, Sara Catalano, Robert J. Green, Marta Gibert, Raoul Scherwitzl, Yaobo Huang, Vladimir N. Strocov, Pavlo Zubko, Shadi Balandeh, Jean-Marc Triscone, George Sawatzky, and Thorsten Schmitt, "Ground-state oxygen holes and the metalinsulator transition in the negative charge-transfer rare-earth nickelates," Nature Communications **7**, 13017 (2016).

[13] G. Fabbris, D. Meyers, J. Okamoto, J. Pelliciari, A. S. Disa, Y. Huang, Z. Y. Chen, W. B. Wu, C. T. Chen, S. Ismail-Beigi, C. H. Ahn, F. J. Walker, D. J. Huang, T. Schmitt, and M. P. M. Dean, "Orbital engineering in nickelate heterostructures driven by anisotropic oxygen hybridization rather than orbital energy levels," Physical Review Letters **117**, 147401 (2016).

[14] Jason D. Hoffman, Brian J. Kirby, Jihwan Kwon, Gilberto Fabbris, D. Meyers, John W. Freeland, Ivar Martin, Olle G. Heinonen, Paul Steadman, Hua Zhou, Christian M. Schlepütz, Mark P. M. Dean, Suzanne G. E. te Velthuis, Jian-Min Zuo, and Anand Bhattacharya, "Oscillatory Noncollinear Magnetism Induced by Interfacial Charge Transfer in Superlattices Composed of Metallic Oxides," Physical Review X **6**, 041038 (2016).